Available online at www.sciencedirect.com
ScienceDirect
Trans. Nonferrous Met. Soc. China 34(2024) 2328−2341
Transactions of Nonferrous Metals Society of China
www.tnmsc.cn

DFT study of sulfidization mechanism of cerussite ($PbCO_3$) and smithsonite ($ZnCO_3$)

Ye CHEN[1,2], Xiao-qin TANG[3], Jian-hua CHEN[1], Meng LIU[4]

1. State Key Laboratory of Featured Metal Materials and Life-cycle Safety for Composite Structures, Guangxi Higher School Key Laboratory of Minerals Engineering, School of Resources, Environment and Materials, Guangxi University, Nanning 530004, China;
2. Key Laboratory of Green Separation and Enrichment of Strategic Metal Mineral Resources, Kunming 650093, China;
3. School of Chemistry and Chemical Engineering, Guangxi University, Nanning 530004, China;
4. Low-carbon Technology and Chemical Reaction Engineering Laboratory, School of Chemical Engineering, Sichuan University, Chengdu 610065, China

Received 16 February 2023; accepted 23 July 2023

Abstract: The differences in the sulfidization mechanism of cerussite ($PbCO_3$) and smithsonite ($ZnCO_3$) were comparatively studied by the density functional theory (DFT) method. Pb−S/Zn−S layers over $PbCO_3$/$ZnCO_3$ surfaces are constructed to simulate the sulfidization structure. The results of layer distance and Mulliken charge suggest that Pb−S layer formed over $PbCO_3$ is stable but Zn−S layer formed over $ZnCO_3$ is unstable. Because of the high covalency of Pb−S layer and the high ionicity of Zn−S layer, the sulfidization−xanthate method is effective for cerussite but ineffective for smithsonite flotation. To recover smithsonite, strong ionicity collectors are required, and hence the sulfidization−amine method is applied more to smithsonite flotation. These differences in the sulfide layer structure and flotation behavior of $PbCO_3$ and $ZnCO_3$ surfaces are mainly attributed to the different polarizabilities of the metal ions (Pb^{2+} and Zn^{2+}) and the ligands (O ligand and S ligand) and the inertness of Zn^{2+} $3d^{10}$ orbital.

Key words: density functional theory; cerussite; smithsonite; sulfidization−xanthate method; sulfidization−amine method

1 Introduction

Lead and zinc metals rank front in world metal consumption and are widely applied in modern industry, which is of great importance [1,2]. They also show similar mineral resource forms, both consisting mainly of sulfide and oxide minerals. Lead and zinc metals are commercially produced from corresponding sulfide minerals by applying the conventional beneficiation and metallurgical techniques [3]. However, with the depletion of easy-recovered sulfide minerals, the effective utilization of lead and zinc oxide minerals has shown tremendous importance in recent years.

Oxide minerals such as cerussite ($PbCO_3$) and smithsonite ($ZnCO_3$) exhibit much greater surface solubility and hydrophilicity than corresponding sulfide minerals, galena (PbS) and sphalerite (ZnS). Hence, direct flotation by using the traditional collectors to make mineral surface hydrophobic is less effective for the recovery of cerussite and

Corresponding author: Jian-hua CHEN, Tel: +86-13737073696, E-mail: jhchen@gxu.edu.cn;
Meng LIU, Tel: +86-18878975372, E-mail: 2713029417@qq.com
DOI: 10.1016/S1003-6326(24)66544-1

smithsonite [4,5]. Surface sulfidization treatment is a common means used in cerussite and smithsonite flotation by further enhancing their surface hydrophobicity via the addition of sulfidizing reagents such as sodium sulfide (Na_2S) or sodium hydrosulfide (NaSH) to allow them to be better recovered by collectors [6,7]. For $PbCO_3$, xanthates are the mostly used collectors, whereas for $ZnCO_3$ amines are used. Therefore, the sulfidization−xanthate and sulfidization−amine methods are widely used in industrial and experimental studies as the most effective methods for cerussite and smithsonite flotation, respectively.

The sulfidization mechanism of lead and zinc oxide minerals has been extensively investigated till now. The results showed that the sulfidization effect could be affected by many factors, such as the dosage of sulfidizing reagents [8] and treatment time [9]. Considerable studies [10−14] also demonstrated that the flotation performance of $PbCO_3$ and $ZnCO_3$ was directly affected by the dosage of Na_2S; excessive concentration could facilitate sulfidization but might hinder collector adsorption on the mineral surface. Many scholars have also done abundant research on sulfidization products using various surface characterization methods, including infrared spectroscopy, Auger electron spectroscopy, X-ray photoelectron spectroscopy (XPS), X-ray diffraction (XRD) and scanning electron microscopy [15−20]. These studies confirmed the formation of sulfide films on sulfidized $PbCO_3$ and $ZnCO_3$ surfaces, and the films were mainly composed of monosulfide and polysulfide [21−23], providing a macro-theoretical basis for the sulfidization mechanism study of $PbCO_3$ and $ZnCO_3$.

Despite the fact that many studies have been conducted for the investigation of sulfidization mechanism, few of them consider the atomic level. In the past decade, the density functional theory (DFT) has been widely used as an effective tool to study the mineral surface properties and mineral−reagent interaction at the atomic level [24−32]. The present DFT studies on the sulfidization mechanism of $PbCO_3$ and $ZnCO_3$ are focused primarily on the adsorption of the hydrolyze of sulfidizing reagents, that is HS^- [33−36]. However, extensive experimental results showed that a layer of Pb/Zn sulfide film was observed on $PbCO_3$/$ZnCO_3$ surface after sulfidization, and hence a model reflecting the formation of the sulfide film is needed to be established.

Recently, more attention has been paid to the coordination chemistry of mineral flotation proposed by CHEN [37,38], and CHEN and ZHU [39], which could be used to precisely describe the interaction between mineral surfaces and reagents/water as the flotation medium. Such interaction can be affected not only by the characteristics of the metal itself but also by the properties of the ligand. Therefore, the above two aspects need to be discussed to compare different sulfidization methods of cerussite and smithsonite.

In the present work, the sulfidization mechanisms of $PbCO_3$ and $ZnCO_3$ were studied comparatively using DFT method. The Pb−S and Zn−S layers were constructed over $PbCO_3$ and $ZnCO_3$ surfaces, respectively, to investigate the effects of sulfidization on the surface structures, electronic properties and surface hydrophobicity. Furthermore, the differences between sulfidization−xanthate method and sulfidization−amine method to recover $PbCO_3$ and $ZnCO_3$ were discussed. It is hoped that the results could give the details about microscopic mechanism of the sulfidization flotation of lead/zinc oxide minerals at the atomic level, and provide theoretical guidance for the molecular design of new and high-efficient collectors in the flotation of lead/zinc oxide minerals.

2 Experimental

2.1 Materials

Cerussite and smithsonite used in the experiments were bought from Yunnan province, China. The X-ray diffraction (XRD) patterns of cerussite and smithsonite are shown in Fig. S1 in Supporting Materials (SM). The bulk mineral was ground and screened to obtain samples with a particle size of 38−76 μm for micro-flotation tests. Reagents used in the experiments were purchased from commercial sources with analytical purity.

2.2 Contact angle measurements

Bulk samples of cerussite and smithsonite were cut into a 2 cm × 3 cm tablet, respectively. Then, one of the surfaces was polished to minimize surface oxidation. To sulfidize the sample, the polished surface was immersed in 1×10^{-3} mol/L

Na_2S solution for 2 h. A water droplet with a volume of 3 μL was then contacted with the sample. The contact angle was determined by recording an image of the prepared sample with the water droplet. Three tests were run under the same conditions, and averages were reported.

2.3 Micro-flotation tests

Micro-flotation tests were carried out by an XFGCII air-filled hanging tank flotation machine (Changchun Exploring Machinery Factory, China). The specific flotation process is shown in Fig. S2 in SM. The concentrates and tailings were filtrated, dried and weighed for calculating the recovery. The calculation formula is

$$R=\frac{m_c}{m_c+m_t}\times 100\% \quad (1)$$

where R is the recovery of minerals, m_c is the mass of the concentrates, and m_t is the mass of the tailings.

2.4 Models and computational details

The geometry optimization of both clean and sulfidized $PbCO_3$ and $ZnCO_3$ surfaces and the surface adsorption of water and collectors were performed through DMol^3 module in the Materials Studio Program [40,41]. Generalized gradient approximation (GGA) with Perdew-Wang's 1991 (PW91) functional was adopted to approximatively treat the exchange−correlation energy. The DFT semicore pseudopots (DSPP) method was employed to treat the core electrons and the localized double numerical basis sets with polarization function (DNP) were used in the calculations. For self-consistent field (SCF) efficient convergence, the direct inversion in an iterative subspace (DIIS) was 6 and thermal smearing of 0.01 was chosen. The convergence thresholds for the geometry optimization and energy calculation were set to (1) maximum energy change of 1×10^{-4} Ha, (2) maximum force of 0.02 Ha/Å (1 Ha=27.21 eV), and (3) maximum displacement of 0.05 Å, respectively.

The PbS (100), ZnS (110) and $ZnCO_3$ (101) surfaces were chosen due to their lowest surface energy, and the corresponding surfaces were cleaved based on the optimized bulk structure. In addition, Fig. 1 demonstrated the geometry configuration of PbS(100) and $PbCO_3$(001) surface. As shown, PbS (100) surface presented an inverted tetragonal pyramid structure with a five-coordinated Pb atom. Thus, the $PbCO_3$ (001) surface with the same five-coordinated tetragonal pyramid structure was chosen in this work. And then, the sulfidized $PbCO_3$ and $ZnCO_3$ surfaces were established by replacing the O atoms with S atoms on $PbCO_3$ and $ZnCO_3$ surfaces.

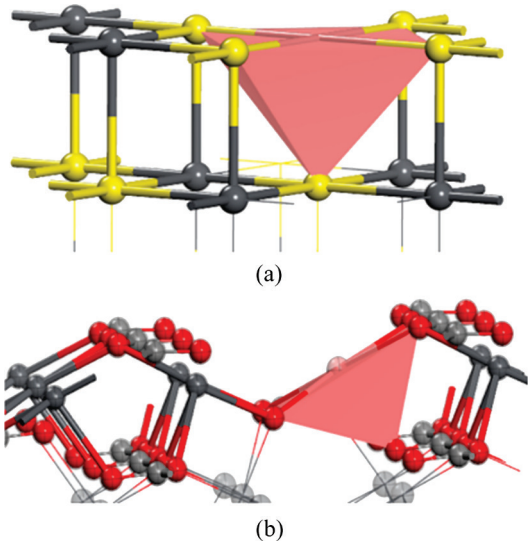

Fig. 1 Inverted tetragonal pyramid structure of PbS (100) surface (a) and $PbCO_3$ (001) surface (b)

After testing the stability of the slab thickness, five atomic layers of PbS and $PbCO_3$ slabs and six atomic layers of ZnS and $ZnCO_3$ slabs were chosen, respectively. To hinder the mirror effect, all supercell slabs were separated by 15 Å of vacuum. As shown in Figs. 2(a−d), the supercell of (2×3×1) PbS (100), (2×3×1) $PbCO_3$ (001), (2×3×1) ZnS (110), and (2×3×1) $ZnCO_3$ (101) surfaces were constructed, and the sulfidized $PbCO_3$ (001) (abbreviated as sul-$PbCO_3$) and sulfidized $ZnCO_3$ (101) (abbreviated as sul-$ZnCO_3$) surfaces were presented in Figs. 2(e−f).

Collectors, butyl xanthate (BX, $CH_3(CH_2)_3OCS_2H$), dodecylamine (DDA, $CH_3(CH_2)_{11}NH_2$), dodecyl secondary amine (DSA, $CH_3(CH_2)_{10}NHCH_3$) and dodecyl tertiary amine (DTA, $CH_3(CH_2)_9N(CH_3)_2$) molecules were optimized in a 15 Å × 15 Å × 15 Å cubic cell using the same parameter setting. The adsorption energy can be expressed by the following equation:

$$\Delta E_{ads}=E_{surf+adsorbate}-E_{surf}-E_{adsorbate} \quad (2)$$

where ΔE_{ads} denotes the adsorption energy, $E_{surf+adsorbate}$ is the total energy of the surface with

the adsorbate, E_{surf} represents the energy of the mineral surface, and $E_{adsorbate}$ is the energy of the adsorbate.

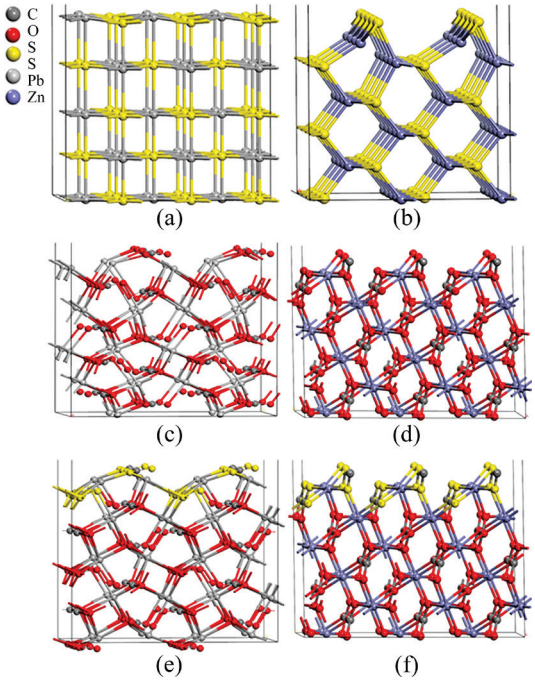

Fig. 2 Models of PbS (100) surface (a), ZnS (110) surface (b), clean $PbCO_3$ (001) surface (c), clean $ZnCO_3$ (101) surface (d), sul-$PbCO_3$ (001) surface (e) and sul-$ZnCO_3$ (101) surface (f)

3 Results and discussion

3.1 Surface structures and electronic properties of $PbCO_3$ and $ZnCO_3$ surfaces before and after sulfidization

Figures 3(a−c) show the optimized geometries of clean $PbCO_3$ surface, sulfidized $PbCO_3$ (abbreviated as sul-$PbCO_3$, representing the Pb−S layer formed over $PbCO_3$ surface) surface and PbS surface, respectively. And the optimized geometries of clean $ZnCO_3$ surface, sulfidized $ZnCO_3$ (abbreviated as sul-$ZnCO_3$, representing the Zn−S layer formed over $ZnCO_3$ surface) surface and ZnS surface are demonstrated in Figs. 4(a−c), respectively. The average bonding distance and coordination number of these six surfaces are listed in Table 1. As shown in Fig. 3(a), for $PbCO_3$ surface, the surface Pb1 atom coordinates with five neighboring O (O1−O5) atoms to form an inverted tetragonal pyramid structure. The exposed Pb1 atom on sul-$PbCO_3$ surface is located at the center of the rectangle, and the Pb—O average bonding

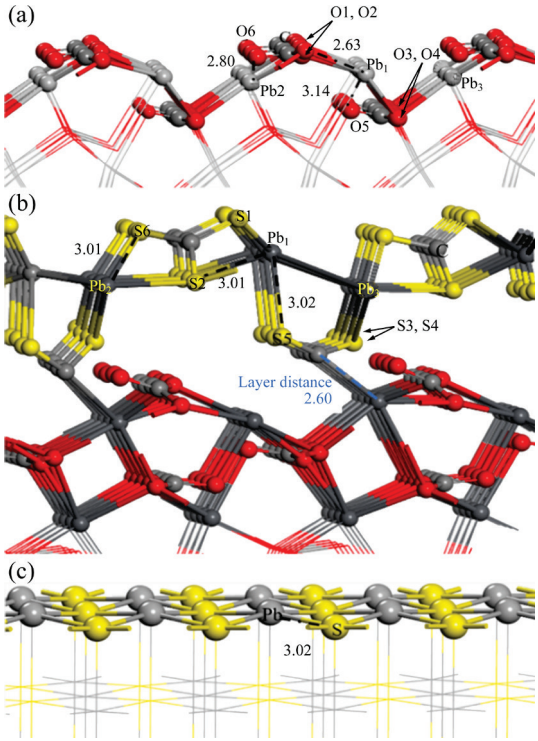

Fig. 3 Optimized geometries of clean $PbCO_3$ (001) surface (a), sul-$PbCO_3$ (001) surface (b) and PbS (100) surface (c) (The distance unit is Å)

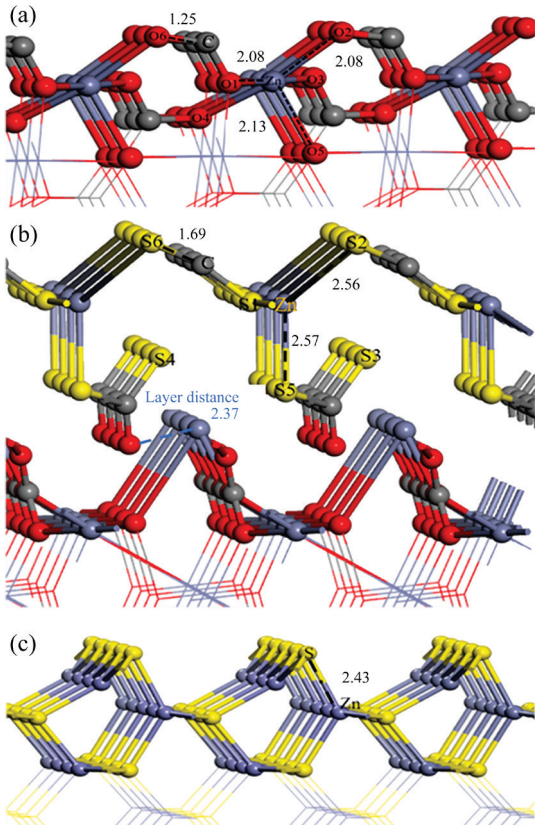

Fig. 4 Optimized geometries of clean $ZnCO_3$ (101) surface (a), sul-$ZnCO_3$ (101) surface (b) and ZnS (110) surface (c) (The distance unit is Å)

distance is 3.02 Å, which is larger than the sum of the atomic radius of Pb and O atoms (2.41 Å). The cleavage of the surface results in an obvious relaxation that causes large displacements of the surface atoms from their bulk positions. The relaxation results in an unstable $PbCO_3$ surface, and consequently, the oxide surface is more likely to be sulfidized by Na_2S.

After sulfidization, a Pb−S layer is formed on $PbCO_3$ surface as shown in Fig. 3(b). The Pb2—S6 and Pb1—S (S1−S5) bonding distances are 3.01−3.02 Å. Although they are larger than the sum of Pb−S atomic radius (2.79 Å), which are significantly smaller than the maximum Pb−S bonding distances (3.21 Å) on the surface. In addition, Pb atom on the first layer of the Pb−S layer could bond with the second layer C atom of the substrate $PbCO_3$ structure to form a Pb—C bond with a layer distance of 2.60 Å, which is very close to the sum of Pb−C atomic radius (2.52 Å). The above results suggest that the Pb−S layer formed over $PbCO_3$ surface is stable.

Meanwhile, Pb2 atom on $PbCO_3$ surface is surrounded by C, O1, O2 and O6 atoms, where O6 atom is located right above Pb2 atom, impeding the adsorption of reagents on Pb2 atom and thus exhibiting steric hindrance. After sulfidization, Pb2 atom becomes surrounded by C, S1, S2 and S6 atoms, where Pb2 atom has been exposed to reagents, and thus steric hindrance is eliminated. Eventually, sul-$PbCO_3$ surface turns more active. Compared with PbS surface shown in Fig. 3(c), the Pb—S average bonding distance is 3.02 Å, which is almost the same as the Pb—S bonding distance on sul-$PbCO_3$ surface (3.01 Å).

As shown in Table 1, the coordination number of surface Pb atom on both PbS and $PbCO_3$ surfaces are the same (five-coordinated). The sulfidization treatment reduces the Pb coordination number from five-coordinated to three-coordinated. Compared with clean surface, the decreased coordination number can make surface Pb atom more exposed to reagents and thus reduce the steric hindrance effect, indicating that collectors could be more easily adsorbed on the sulfidized $PbCO_3$ surface. The results also suggest that the Pb−S layer can bond stably on the substrate $PbCO_3$ structure.

As shown in Fig. 4 and Table 1, the surface Zn atom and five nearby O (O1−O5) atoms form an inverted tetragonal pyramid structure (see Fig. 4(a)) and the coordination number of Zn atom is 5 (see Table 1). The average Zn—O bonding distance on $ZnCO_3$ surface is 2.10 Å. After sulfidization, Zn atom bonds with S1, S2 and S5 atoms while S3 and S4 atoms bond with C atom (see Fig. 4(b)), resulting in a decrease of surface Zn coordination number from five-coordinated to three-coordinated (see Table 1). Zn atom on ZnS surface is also three-coordinated (see Fig. 4(c) and Table 1). The distance of Zn—S bond on sul-$ZnCO_3$ surface is 2.57 Å, close to the Zn—S bonding distance on ZnS surface (2.43 Å). The results demonstrate the similar geometric structures between sul-$ZnCO_3$ surface and ZnS surface.

Furthermore, sulfidization treatment disconnects the Zn—O bond between the first layer O atom on the Zn−S layer and the second layer Zn atom on the substrate $ZnCO_3$ structure with a layer distance of 2.37 Å, which is larger than not only the sum of Zn−O atomic radius (1.99 Å) but also the Zn—O bonding distance on $ZnCO_3$ surface (2.13 Å), demonstrating that the Zn−S layer formed on $ZnCO_3$ surface is relatively unstable.

The above analysis of geometric structure

Table 1 Average bonding distance and coordination number of different surfaces

Surface	Average bonding distance/Å						Coordination number	
	Pb—O	Zn—O	Pb—S	Zn—S	O—C	S—C	Metal−O	Metal−S
Clean $PbCO_3$	2.62	−	−	−	1.31	−	5	−
sul-$PbCO_3$	2.55	−	3.01	−	1.29	1.73	−	3
PbS	−	−	3.02	−	−	−	−	5
Clean $ZnCO_3$	−	2.16	−	−	1.31	−	5	−
sul-$ZnCO_3$	−	2.18	−	2.48	1.31	1.74	−	3
ZnS	−	−	−	2.43	−	−	−	3

suggests that the Pb−S layer formed over $PbCO_3$ surface is stable, whereas the Zn−S layer formed over $ZnCO_3$ surface is relatively unstable. This might pose different impacts on the subsequent reagent adsorption.

According to the coordination chemistry of mineral flotation [37−39], Pb^{2+} interacting with either O ligand or S ligand is in accordance with the close-packing principle. Since the outer shell electron distribution of Pb^{2+} is $6s^26p^0$, which has at most three unoccupied orbitals, and thus Pb^{2+} cannot provide sufficient hybrid orbitals for coordination. Therefore, the charge and radius effect is dominant in lead complexes. Moreover, Pb^{2+} is of great polarizability, which enhances the interaction between Pb^{2+} and the ligand. The polarizability of S ligand is greater than that of O ligand, and hence Pb−S layer formed after sulfidization exhibits higher polarizability and is structurally more stable. However, the outer shell electron distribution of Zn^{2+} is $3d^{10}4s^04p^0$. Zn^{2+} presents small polarizability, while S has higher polarizability and thus shows a strong attraction to electrons. Hence, the orbital hybridization mode of Zn−S is sp^3d^2 outer-orbital hybridization, forming an outer-orbital complex. The outer-orbital coordination is orientational and covalent, and the effect is weak, so the Zn−S layer formed after sulfidization is unstable. Furthermore, the instability of sul-$ZnCO_3$ surface has also been demonstrated by BAI et al [15].

To further investigate the effect of sulfidization on the mineral surface, the electronic property is investigated. The atom Mulliken charge of those six different mineral surfaces is listed in Table 2. For Pb atom, the values of Mulliken charge decrease from 0.71*e* on $PbCO_3$ surface to 0.36*e* on sul-$PbCO_3$ surface. The sulfidization leads to charge transfer from Pb atom to S atom. The Pb atom Mulliken charge on sul-$PbCO_3$ surface is very close to that on PbS surface (0.38*e*), indicating that sul-$PbCO_3$ surface exhibits strong covalency.

For smithsonite, the Zn atom Mulliken charge is 0.75*e* on $ZnCO_3$ surface. Unlike sul-$PbCO_3$ surface, the Zn atom Mulliken charge on sul-$ZnCO_3$ surface (0.38*e*) is greater than that on ZnS surface (0.29*e*), suggesting that sul-$ZnCO_3$ surface could bind electrons more strongly, exhibiting stronger ionicity.

Consequently, xanthates are more readily to adsorb on the surface with strong covalency, and thus xanthates are easy to interact with sul-$PbCO_3$ surface but are relatively hard to interact with sul-$ZnCO_3$ surface. Hence, for the sulfidization flotation of $ZnCO_3$, collectors with strong ionicity such as amines should be further investigated.

Table 2 Mulliken charge of mineral surface atoms

Mineral surface	Mulliken charge/*e*				
	Pb	Zn	O	S	C
Clean $PbCO_3$	0.71	−	−0.44	−	0.65
sul-$PbCO_3$	0.36	−	−	−0.23	0.22
PbS	0.38	−	−	−0.40	−
Clean $ZnCO_3$	−	0.75	−0.41	−	0.36
sul-$ZnCO_3$	−	0.38	−	−0.17	0.08
ZnS	−	0.29	−	−0.27	−

3.2 Adsorption of water molecules on $PbCO_3$ and $ZnCO_3$ surfaces before and after sulfidization

It is well acknowledged that floatability depends on the hydrophobicity of mineral surfaces. $PbCO_3$ and $ZnCO_3$ surfaces are hydrophilic. In order to investigate the effect of sulfidization on the wettability of $PbCO_3$ and $ZnCO_3$, the contact angle measurements are carried out, as shown in Fig. S3 in SM. The contact angles of clean $PbCO_3$ surface and clean $ZnCO_3$ surface are 49.8º and 38.6º, respectively, suggesting that both surfaces are hydrophilic and clean $ZnCO_3$ surface is slightly more hydrophilic than clean $PbCO_3$ surface. However, after sulfidization treatment, the contact angles of sul-$PbCO_3$ surface and sul-$ZnCO_3$ surface are changed to 77.2° and 67.1°, respectively, indicating that both surfaces become more hydrophobic after sulfidization treatment.

Moreover, the adsorptions of a single water molecule on clean $PbCO_3$ surface (Fig. 5(a)), sul-$PbCO_3$ surface (Fig. 5(b)), clean $ZnCO_3$ surface (Fig. 5(c)), and sul-$ZnCO_3$ surface (Fig. 5(d)) are studied, respectively. Before sulfidization, for $PbCO_3$, the interaction distance between surface Pb atom and water O atom is 2.43 Å, which is very close to the sum of the atomic radius of Pb and O atom (2.41 Å). The calculated adsorption energy is –80.25 kJ/mol. For $ZnCO_3$, the interaction distance between surface Zn atom and water O atom is 1.97 Å, which is slightly less than the sum of the atomic radius of Zn and O atom (1.99 Å). The

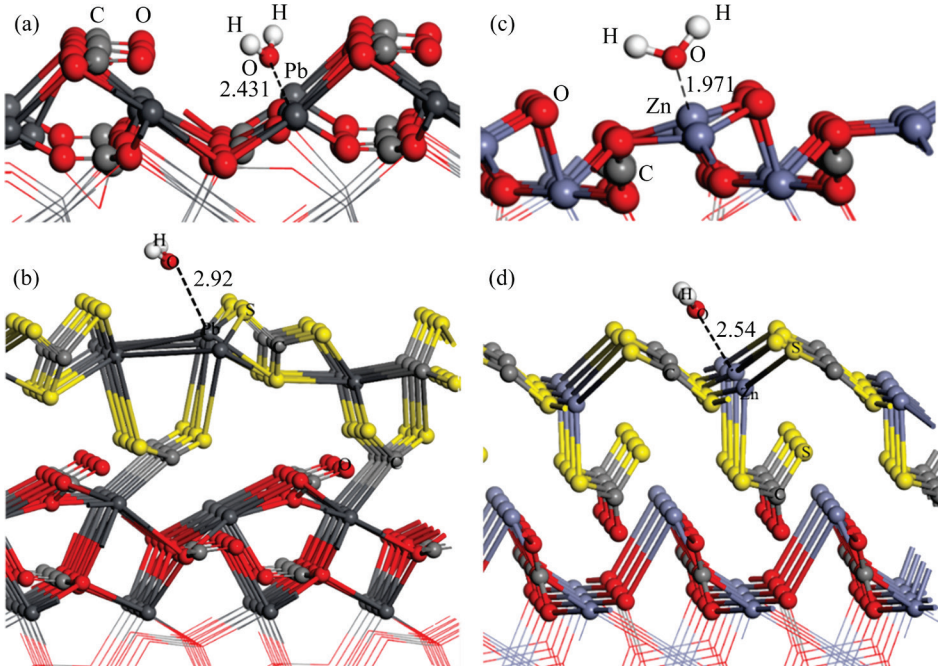

Fig. 5 Optimized geometries of single H_2O molecule adsorbed on clean $PbCO_3$ surface (a), sul-$PbCO_3$ surface (b), clean $ZnCO_3$ surface (c) and sul-$ZnCO_3$ surface (d) (The distance unit is Å)

adsorption energy is –100.92 kJ/mol. These results suggest that the H_2O molecule could strongly adsorb on both $PbCO_3$ and $ZnCO_3$ surfaces, and $ZnCO_3$ surface might be more hydrophilic than $PbCO_3$ surface. From the perspective of the coordination chemistry of mineral flotation [37−39], the outer shell of Pb^{2+} has one pair of lone pair electrons on the 6s orbital, which would perform repel effect on the ligand (i.e. water molecules). This further explains why the surface of $ZnCO_3$ is more hydrophilic than that of $PbCO_3$.

After sulfidization, for $PbCO_3$, the interaction distance between surface Pb atom and water O atom increases to 2.92 Å, which is far larger than the Pb—O bonding distance, and the adsorption energy (−72.96 kJ/mol) is more positive than that on $PbCO_3$ surface (−80.25 kJ/mol), suggesting that the newly formed Pb−S layer could increase the hydrophobicity of $PbCO_3$. Similarly, for $ZnCO_3$, the interaction distance (2.54 Å) between surface Zn atom and water O atom also far exceeds the Zn—O bonding distance; however, the adsorption energy is –69.12 kJ/mol, which is significantly less negative than that on $ZnCO_3$ surface (–100.92 kJ/mol), which indicates that the surface turns to be more hydrophobic after sulfidization.

The above results demonstrate that the sulfidization treatment via forming a layer of sulfide structure over the oxide surface makes lead/zinc oxide mineral surfaces more hydrophobic. For both $PbCO_3$ and $ZnCO_3$, before sulfidization, metal ions (i.e. Pb^{2+} and Zn^{2+}) coordinate with O ligand with a relatively high electronegativity of 3.44 to form ionic bonds. However, after sulfidization, metal ions come to coordinate with S ligand which has a lower electronegativity of 2.58. According to the coordination chemistry of mineral flotation [37−39], the decreased electronegativity of the ligand leads to the increase of polarizability, and thus the enhancement of the nephelauxetic effect of metal ions. The increased nephelauxetic effect of metal ions results in stronger covalent bonding between the metal ion and the ligand, and hence both $PbCO_3$ and $ZnCO_3$ become more hydrophobic after sulfidization treatment.

3.3 Adsorption of xanthate on $PbCO_3$ and $ZnCO_3$ surfaces before and after sulfidization

The sulfidization−xanthate method is most widely used in industry for oxide mineral beneficiation and butyl xanthate (BX) is the commonly used collector. Thus, the adsorption of BX on clean and sul-$PbCO_3$/$ZnCO_3$ surfaces is studied. The optimized adsorption geometries of BX adsorbed on clean and sul-$PbCO_3$ surfaces are shown in Figs. 6(a−b). On $PbCO_3$ surface, the

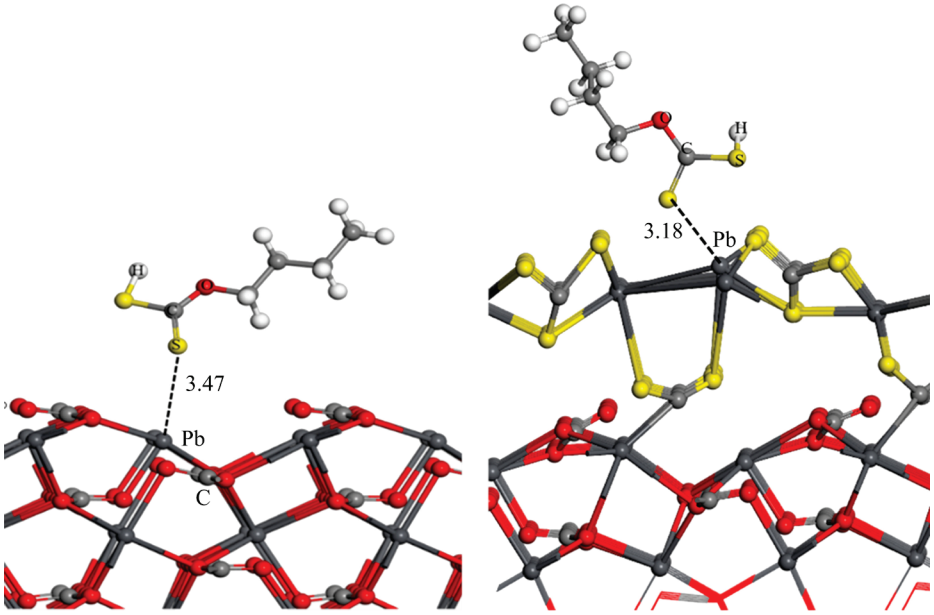

Fig. 6 Optimized geometry of BX adsorbed on clean $PbCO_3$ (001) surface (a) and sul-$PbCO_3$ (001) surface (b) (The distance unit is Å)

interaction distance of surface Pb atom and xanthate S atom is 3.47 Å, which is greater than the sum of Pb−S atomic radius (2.79 Å). The adsorption energy (–78.27 kJ/mol) is comparable to that of water adsorbed on $PbCO_3$ surface (–80.25 kJ/mol), suggesting weak adsorption between BX and $PbCO_3$ surface. After sulfidization, the surface Pb atom bonds to xanthate S atom with a distance of 3.18 Å and the adsorption energy decreases to −112.40 kJ/mol, which is far less negative than the adsorption energy of water adsorbed on sul-$PbCO_3$ surface (−72.96 kJ/mol). The results demonstrate that BX could strongly adsorb on sul-$PbCO_3$ surface.

To further study the sulfidization−xanthate mechanism, the density of states (DOS) of sulfidized surface Pb atom (Surface-Pb) and xanthate S atom (Xanthate-S) before and after the interaction with BX is calculated, and the results are shown in Fig. 7. Before adsorption, xanthate S 3s orbital is located at the deeper energy level (from −14 to −12 eV). Near Fermi level (E_F), S 3p, Pb 6p and partial Pb 6s orbitals occupy the high energy levels, indicating that these orbitals are more likely to involve in the interaction. After adsorption, there exists an obvious electron state overlap between Pb 6s and S 3p orbitals at the energy range from −6 to 0 eV. The antibonding DOS peaks resonate from

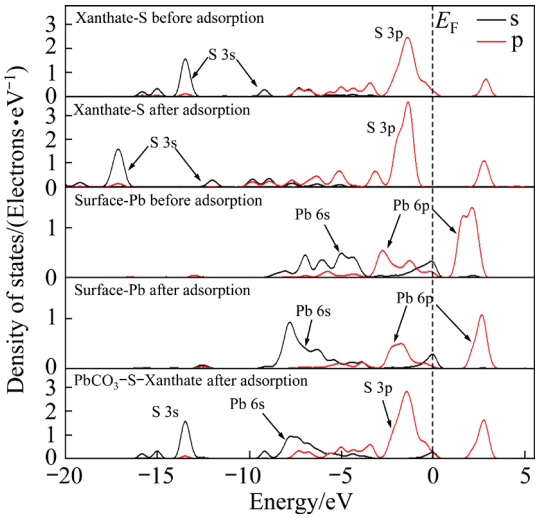

Fig. 7 DOS of xanthate S atom and sulfidized surface Pb atom before and after interaction with BX (E_F is set at zero energy)

−8 to −6 eV, which is much more localized. The result confirms a great Pb—S bonding interaction between xanthate and sul-$PbCO_3$. The sulfide layer formed over $PbCO_3$ surface shows great reactivity to BX.

Figure 8 presents the optimized geometries of BX adsorbed on clean $ZnCO_3$ and sul-$ZnCO_3$ surfaces. The adsorption energies of BX on clean and sul-$ZnCO_3$ surface are −76.89 and −92.85 kJ/mol, respectively. However, the interaction distances

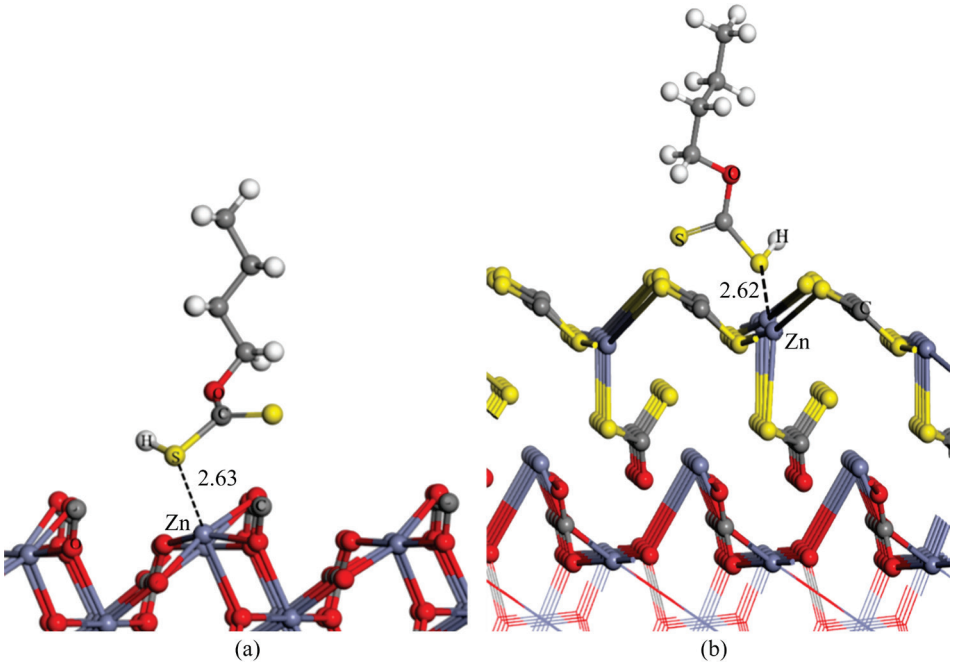

Fig. 8 Optimized geometries of BX adsorbed on clean $ZnCO_3$ (101) surface (a) and sul-$ZnCO_3$ (101) surface (b) (The distance unit is Å)

between xanthate S atom and clean/sulfidized surface Zn atom are 2.63 Å/2.62 Å, far greater than the sum of Zn−S atomic radius (2.37 Å). Furthermore, as mentioned above, the Zn−S layer formed over $ZnCO_3$ surface is relatively unstable. These results indicate that although sulfidization treatment could enhance the interaction between BX and $ZnCO_3$ to some extent, the sulfidization−xanthate method is ineffective for smithsonite flotation.

Figure 9 shows the DOS of xanthate S atom (Xanthate-S) and sulfidized surface Zn (Surface-Zn) atom before and after the interaction with BX. Before the interaction, S 3p orbital occupies high energy levels near E_F. Zn 3d orbital is localized from −5 to −4 eV, which shows weak reactivity of surface Zn atom. After the interaction, these DOS peaks shift to deeper energy levels, indicating greater stability of these atoms. Zn 3d orbital hardly overlaps with S 3p orbital, demonstrating that BX rarely interacts with sul-$ZnCO_3$ surface. This further explains that the sulfidization−xanthate method is ineffective for $ZnCO_3$.

At pH 9, when using 1×10^{-3} mol/L BX as the collector, the influence of Na_2S dosage on the flotation of cerussite and smithsonite is shown in Fig. 10. As shown, the recovery of cerussite increases significantly from 43.50% to 78.50% as

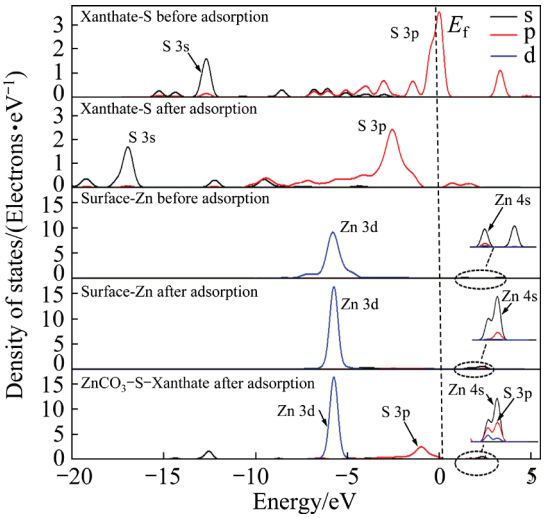

Fig. 9 DOS of xanthate S atom and sulfidized surface Zn atom before and after interaction with BX (E_F is set at zero energy)

the Na_2S dosage is increased from 1×10^{-6} to 1×10^{-5} mol/L. With the further increase of Na_2S dosage, the recovery of cerussite decreases gradually. However, for smithsonite, the dosing of Na_2S has little effect on its recovery. These flotation results further prove that the sulfidization−xanthate method is effective for cerussite flotation but less effective for smithsonite flotation.

It is worth noting that the coordination of xanthates is dominated by π-backbonding. The d

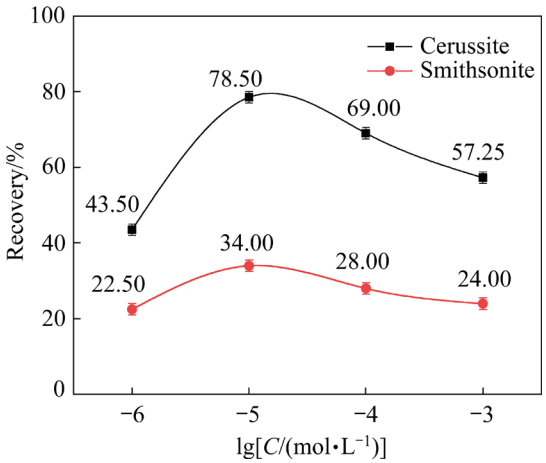

Fig. 10 Effect of Na_2S dosage (C) on flotation of cerussite and smithsonite when using 1×10^{-3} mol/L BX as collector (pH=9)

orbital configuration of Zn^{2+} is d^{10}. Although Zn^{2+} has π electrons that can form π-backbonds with unoccupied π orbitals of xanthates, the d^{10} configuration is structurally stable with poor orbital activity and weak bonding ability, the interaction of Zn^{2+} with BX is thus relatively weak. In addition, different bonds of organic compounds have different polarizabilities. The higher the polarizability of the bonds, the more the electron-cloud overlap between the bonds and metal ions, to form covalent bonds. This is of great significance for the adsorption of reagents on mineral surfaces. The polarization of the C═S double bond in xanthates is very high (43.7×10^{-25} cm^3) [37], indicating that the C═S double bond in xanthates has strong covalent ability and is easy to form coordination bonds with transition metals. Referring back to Table 2, the Mulliken charges of Pb atom on sul-$PbCO_3$ surface (0.36e) and PbS surface (0.38e) are similar, whereas the Mulliken charge of Zn atom on sul-$ZnCO_3$ surface (0.38e) is greater than that on ZnS surface (0.29e). These results indicate that sul-$ZnCO_3$ surface has a greater ionicity than sul-$PbCO_3$ surface. Hence, to effectively float smithsonite, collectors with strong ionicity should be used.

3.4 Adsorption of amine on $ZnCO_3$ surface after sulfidization

For smithsonite flotation, the sulfidization−amine method is commonly applied in industry. As amines are ionic collectors, the differences in the interaction mechanism between sulfidization−xanthate and sulfidization−amine to float the smithsonite should be investigated. Amines with 12 carbon atoms are the most common collectors for smithsonite flotation, and thus, DDA, DSA and DTA are discussed. Amine collectors can provide electrons, while $ZnCO_3$ accepts electrons. Therefore, the highest occupied molecular orbitals (HOMO) of amines are calculated in Fig. 11. As shown, the electrons are concentrated almost exclusively on the amino groups of three reagents. The methyl group is the electron-withdrawing group, and hence electrons could be prone to transferring from the amino group to the methyl group. For DSA and DTA with increasing methyl groups, the energy values of HOMO orbitals turn more positive, and consequently, the HOMO orbitals of DDA have the lowest energy value of −0.19 eV among these three reagents. It is known that the electron affinity of reagents (i.e. the ability to donate electrons) increases with the decrease of the energy value of HOMO; therefore, DDA shows the strongest electron affinity, and hence is more readily to coordination. Hence, DDA is chosen as the most effective collector in the study of the sulfidization−amine method. This also agrees with the practical situation in industry.

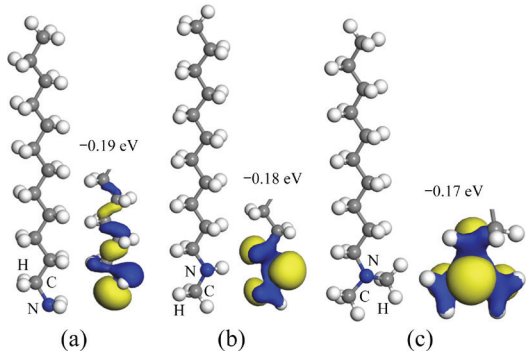

Fig. 11 HOMO of DDA (a), DSA (b) and DTA (c) molecules

To compare the different mechanisms of sulfidization−xanthate and sulfidization−amine methods, the adsorption of DDA on sul-$ZnCO_3$ surface is studied. The optimized geometry configuration is shown in Fig. 12. After the interaction, there is a new Zn—N bond formed with a bonding distance of 1.95 Å, which is slightly less than the sum of Zn−N atomic radius (2.03 Å). The adsorption energy is –233.66 kJ/mol. Compared with the adsorption energy of xanthate on

sul-$ZnCO_3$ surface (–92.85 kJ/mol), the adsorption of DDA on sul-$ZnCO_3$ surface is much stronger. The results demonstrate that the sulfidization−amine method can be used to float smithsonite effectively.

Figure 13 shows the DOS of DDA N atom (Dodethyl amine-N) and sulfidized surface Zn atom (Surface-Zn) before and after DDA adsorption. Before adsorption, N 2p orbital is located at an extensive energy range from −17 to 0 eV. This orbital is also observed near E_F, indicating that N 2p orbital is more likely to be involved in the mineral−reagent interaction. After amine adsorption, the DOS of N and Zn atoms are changed dramatically.

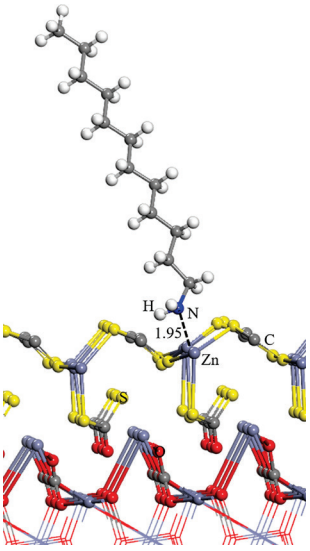

Fig. 12 Adsorption configuration of DDA on sul-$ZnCO_3$ (101) surface

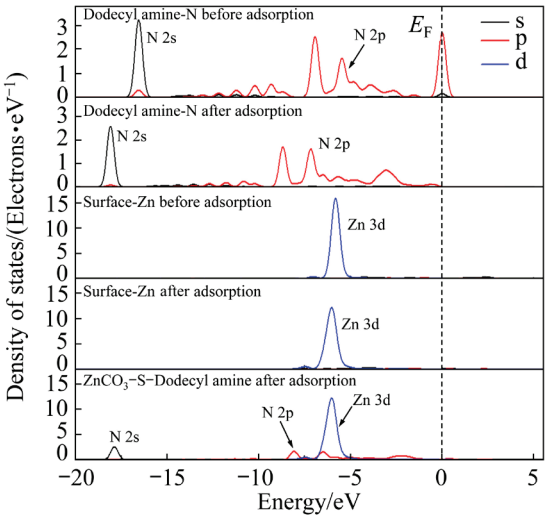

Fig. 13 DOS of amine N atom and sulfidized surface Zn atom before and after interaction with DDA (E_F is set at zero energy)

The DOS peak of Zn 3d orbital shifts from the energy range from −5 to −3 eV to a deeper energy level from −7 to −5 eV. The DOS peak value of N 2p orbital obviously decreases from 2.7 to 1.9 eV, demonstrating that DDA N atom is more stable after amine adsorption. Different from xanthate adsorption, there exists an obvious electron state overlap between Zn 3d and N 2p orbitals within the energy range from −7 to −5 eV. The results suggest that the interaction between DDA and sul-$ZnCO_3$ surface is stronger, and the sulfidization−amine method is more effective over smithsonite than the sulfidization−xanthate method.

At pH 9, when using 1×10^{-3} mol/L BX and DDA as the collector, the influence of Na_2S dosage on the flotation of smithsonite is compared in Fig. 14. As shown, the recovery of smithsonite increases gradually from 40.55% to 80.25% as the DDA dosage is increased from 1×10^{-6} to 1×10^{-4} mol/L. With the further increase of DDA dosage, the recovery of smithsonite begins to decline. Compared with using 1×10^{-3} mol/L BX as the collector, the recovery of smithsonite raises significantly from 28.50% to 80.25% when 1×10^{-4} mol/L Na_2S is added. This further proves that for smithsonite flotation the sulfidization−amine method is more effective than the sulfidization−xanthate method.

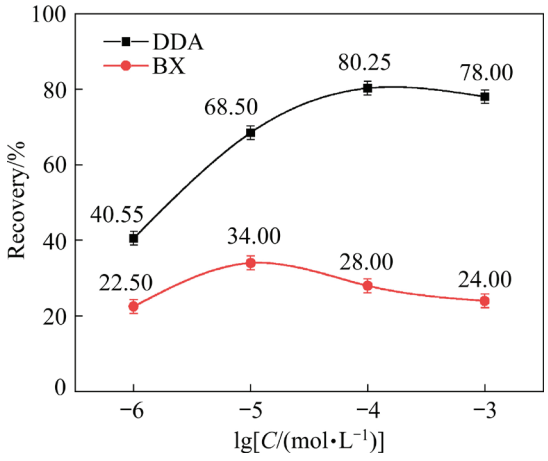

Fig. 14 Effect of Na_2S dosage (C) on flotation of smithsonite when using 1×10^{-3} mol/L BX and DDA as collector (pH=9)

To further investigate the electronic property of sul-$ZnCO_3$ surface, the electron density of DDA adsorbed on sul-$ZnCO_3$ surface is studied. As shown in Fig. 15, the darker the red color, the denser the charge. The electron cover area of

surface S atom is smaller than that of DDA N atom. The increase in electron density between DDA N atom and surface Zn atom demonstrates the strengthening of the polarity of the Zn—N bond. Hence, the adsorption of amine on sul-$ZnCO_3$ is electrostatic adsorption but along with covalent interaction to a certain extent. In summary, the sulfidization−amine mechanism could attribute to the interaction between strong ionicity amine collectors and sul-$ZnCO_3$ surface, while the sulfidization−xanthate mechanism is accepted as strong covalency between sul-$PbCO_3$ surface and xanthate collectors with weak polarity.

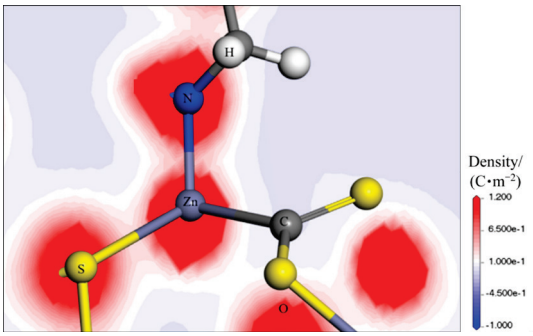

Fig. 15 Contour plots of electron density of DDA adsorbed on sul-$ZnCO_3$ (101) surface

4 Conclusions

(1) Pb^{2+} has a relatively larger polarizability than Zn^{2+}. When Pb^{2+} coordinates with S ligand that has larger polarizability to form the Pb−S layer, showing greater covalency, the Pb−S layer formed over $PbCO_3$ is structurally stable. However, Zn^{2+} coordinates with S ligand to form an outer-orbital complex, the Zn−S layer, with a weak effect. Hence, the Zn−S layer formed over $ZnCO_3$ is structurally unstable.

(2) Both results of layer distance and Mulliken charge confirm that Pb−S layer can bond stably with the substrate $PbCO_3$, showing strong covalency, whereas Zn−S layer bonds unstably with the substrate $ZnCO_3$, presenting strong ionicity. Thus, the sulfidization−xanthate method is only applicable to the recovery of cerussite. To float smithsonite effectively, collectors with strong ionicity such as amines are required, and hence the sulfidization−amine method is preferable for the recovery of smithsonite.

(3) Sulfidization treatment enhances the hydrophobicity of both $PbCO_3$ and $ZnCO_3$ surfaces. This is attributed to the change in ligand type from O ligand to S ligand. The coordination of Pb/Zn with S ligand that has higher polarizability enhances the covalency of sul-$PbCO_3$/$ZnCO_3$ surfaces.

CRediT authorship contribution statement

Ye CHEN: Project administration, Funding acquisition, Formal analysis, Writing − Review and editing; **Xiao-qin TANG:** Investigation, Validation, Visualization, Writing − Review and editing; **Jian-hua CHEN:** Conceptualization, Methodology, Resources; **Meng LIU:** Supervision, Data curation, Writing − Original draft.

Declaration of competing interest

The authors declare that they have no known competing financial interests or personal relationships that could have appeared to influence the work reported in this paper.

Acknowledgments

This work was funded by the National Natural Science Foundation of China (Nos. 52174246, 51864003), and the Open Foundation of Key Laboratory of Green Separation and Enrichment of Strategic Metal Mineral Resources, China (No. 202205AG070012).

Supporting Materials

Supporting Materials in this paper can be found at: http://tnmsc.csu.edu.cn/download/20-p2328-2023-0182-Supporting_materials.pdf.

References

[1] LIU Cheng, ZHANG Wen-cai, SONG Shao-xian, LI Hong-qiang, LIU Yong. Flotation separation of smithsonite from calcite using 2-phosphonobutane-1,2,4-tricarboxylic acid as a depressant [J]. Powder Technology, 2019, 352: 11−15.

[2] SCHRÖDER-WOLTHOORN A, KUITERT S, DIJKMAN H, HUISMAN J L. Application of sulfate reduction for the biological conversion of anglesite ($PbSO_4$) to galena (PbS) [J]. Hydrometallurgy, 2008, 94(1/2/3/4): 105−109.

[3] KURSUNOGLU S, TOP S, KAYA M. Recovery of zinc and lead from Yahyali non-sulphide flotation tailing by sequential acidic and sodium hydroxide leaching in the presence of potassium sodium tartrate [J]. Transactions of Nonferrous Metals Society of China, 2020, 30(12): 3367−3378.

[4] FUERSTENAU M C, OLIVAS S A, HERRERA-URBINA R, HAN K N. The surface characteristics and flotation behavior of anglesite and cerussite [J]. International Journal of Mineral Processing, 1987, 20(1/2): 73−85.

[5] HERRERA-URBINA R, SOTILLO F J, FUERSTENAU D W. Effect of sodium sulfide additions on the pulp potential and amyl xanthate flotation of cerussite and galena [J]. International Journal of Mineral Processing, 1999, 55(3): 157−170.

[6] KUCHAR D, FUKUTA T, ONYANGO MS, MATSUDA H. Sulfidization treatment of molten incineration fly ashes with Na_2S for zinc, lead and copper resource recovery [J]. Chemosphere, 2007, 67(8): 1518−1525.

[7] ZHANG Song, WEN Shu-ming, LIANG Guan-yu, XIAN Yong-jun, CHEN Lu-zheng. Ammonia pretreatment for enhancement of Pb ions adsorption on smithsonite surface and its flotation performance [J]. Applied Surface Science, 2022, 590(4): 153069.

[8] HOSSEINI SH, FORSSBERG E. Psicochemical studies of smithsonite flotation using mixed anionic/cationic collector [J]. Minerals Engineering, 2007, 20(6): 621−624.

[9] BAI Xu, LIU Jian, WEN Shu-ming, WANG Yu, LIN Yi-lin. Effect of ammonium salt on the stability of surface sulfide layer of smithsonite and its flotation performance [J]. Applied Surface Science, 2020, 514: 145851.

[10] BAI Shao-jun, LI Chun-long, FU Xiang-yu, LIU Jian, WEN Shu-ming. Characterization of zinc sulfide species on smithsonite surfaces during sulfidation processing: Effect of ammonia liquor [J]. Journal of Industrial and Engineering Chemistry, 2018, 61: 19−27.

[11] FENG Qi-cheng, WEN Shu-ming. Formation of zinc sulfide species on smithsonite surfaces and its response to flotation performance [J]. Journal of Alloys and Compounds, 2017, 709: 602−608.

[12] HERRERA-URBINA R, SOTILLO F J, FUERSTENAU D W. Amyl xanthate uptake by natural and sulfide-treated cerussite and galena [J]. International Journal of Mineral Processing, 1998, 55(2): 113−128.

[13] MALGHAN S G. Role of sodium sulfide in the flotation of oxidized copper, lead, and zinc ores [J]. Minerals and Metallurgical Processing, 1986, 3(3): 158−163.

[14] LIN Hong-fu, WENG Wei, ZHONG Shui-ping, QIU Guan-zhou. Enhanced recovery of zinc and lead by slag composition optimization in rotary kiln [J]. Transactions of Nonferrous Metals Society of China, 2022, 32(9): 3110−3122.

[15] BAI Shao-jun, YU Pan, DING Zhan, LI Chun-long, XIAN Yong-jun, WEN Shu-ming. Ammonium chloride catalyze sulfidation mechanism of smithsonite surface: Visual MINTEQ models, ToF-SIMS and DFT studies [J]. Minerals Engineering, 2020, 146: 106115.

[16] CHEN Jing-hua, ZHANG Fang-qi. Investigation on electrochemical properties of cerussite in sulfidation-flotation system [J]. Mining and Metallurgical Engineering, 2017, 37(4): 38−40. (in Chinese)

[17] LIANG Dong-yun, ZHANG Zhi-xiong, XU Zhi-hua. Relation between the crystallochemical properties and sulphurized behaviours of cerussite and smithsonite [J]. Journal of Guangdong Non-ferrous metals, 1992, 2(2): 83−88. (in Chinese)

[18] LI Jia-lei, LIU Si-yan, LIU Dian-wen, LIU Rui-zeng, LIU Zhi-cheng, JIA Xiao-dong, CHANG Tian-cang. Sulfidization mechanism in the flotation of cerussite: A heterogeneous solid−liquid reaction that yields $PbCO_3$/PbS core−shell particles [J]. Minerals Engineering, 2020, 153: 106400.

[19] LIU Rui-zeng, LIU Dian-wen, LI Jia-lei, LIU Si-yan, LIU Zhi-cheng, GAO Lian-qi, JIA Xiao-dong, AO Shun-fu. Improved understanding of the sulfidization mechanism in cerussite flotation: An XPS, ToF−SIMS and FESEM investigation [J]. Colloids and Surfaces A: Physicochemical and Engineering Aspects, 2020, 595: 124508.

[20] MARABINI A M, CIRIACHI M, PLESCIA P, BARBARO M. Chelating reagents for flotation [J]. Minerals Engineering, 2007, 20(10): 1014−1025.

[21] FENG Qi-cheng, WEN Shu-ming, ZHAO Wen-juan, DENG Jiu-shuai, XIAN Yong-jun. Adsorption of sulfide ions on cerussite surfaces and implications for flotation [J]. Applied Surface Science, 2016, 360: 365−372.

[22] FENG Qi-cheng, WEN Shu-ming, ZHAO Wen-juan, LIU Jian, LIU Dan. Effect of pH on surface characteristics and flotation of sulfidized cerussite [J]. Physicochemical Problems of Mineral Processing, 2016, 52(2): 676−689.

[23] LUO Bin, LIU Quan-jun, DENG Jiu-shuai, YU Li, LAI Hao, SONG Chao, LI Shi-mei. Characterization of sulfide film on smithsonite surface during sulfidation processing and its response to flotation performance [J]. Powder Technology, 2019, 351: 144−152.

[24] CHEN Ye, LIU Xiao-mei, CHEN Jian-hua. Steric hindrance effect on adsorption of xanthate on sphalerite surface: A DFT study [J]. Minerals Engineering, 2021, 165: 106834.

[25] JIA Yun, ZHANG Yu, HUANG Yao-guo, CHEN Lin-lin, WANG Ming, ZHANG Ya-li. Synthesis of trimethylacetyl thiobenzamide and its flotation separation performance of galena from sphalerite [J]. Applied Surface Science, 2021, 569: 151055.

[26] LIU Jian, WEN Shu-ming, DENG Jiu-shuai, CHEN Xiu-min, FENG Qi-cheng. DFT study of ethyl xanthate interaction with sphalerite (110) surface in the absence and presence of copper [J]. Applied Surface Science, 2014, 311: 258−263.

[27] MKHONTO P P, ZHANG Xing-rong, LU Liang, XIONG Wei, ZHU Yang-ge, HAN Long, NGOEPE P E. Adsorption mechanisms and effects of thiocarbamate collectors in the separation of chalcopyrite from pyrite minerals: DFT and experimental studies [J]. Minerals Engineering, 2022, 176: 107318.

[28] QI Jing, LIU Sheng, DONG Yan, LIU Guang-yi. Revealing the role of dithiocarbamate ester group in hydroxamic acid flotation of cassiterite with in situ AFM, DFT and XPS [J]. Applied Surface Science, 2022, 604: 154521.

[29] WU Jie, YANG Bing-qiao, SONG Shao-xian, QUINTANA M, JIA Fei-fei, TIAN Xiang. The efficient recovery of molybdenite fines using a novel collector: Flotation performances, adsorption mechanism and DFT calculation [J]. Minerals Engineering, 2022, 188: 107848.

[30] YANG Xi, LI Yu-qiong, CHEN Jian-hua. DFT study of the occurrence state of In and the correlation of In and Fe in sphalerite [J]. Minerals Engineering, 2022, 183: 107596.

[31] LU Yu-xi, WANG Shuai, CAO Zhan-fang, MA Xin, ZHONG Hong. Structure-activity relationships of oxime compounds as flotation collectors by DFT calculations [J]. Transactions of Nonferrous Metals Society of China, 2022, 32(12): 4076−4087.

[32] MENG Xiao-yu, ZHAO Hong-bo, ZHANG Yi-sheng, WANG Shuai, GU Guo-hua, QIU Guan-zhou. Effects of copper ions on dissolution mechanism of marmatite [J]. Transactions of Nonferrous Metals Society of China, 2022, 32(12): 4099−4112.
[33] FENG Qi-cheng, WEN Shu-ming, DENG Jiu-shuai, ZHAO Wen-juan. Combined DFT and XPS investigation of enhanced adsorption of sulfide species onto cerussite by surface modification with chloride [J]. Applied Surface Science, 2017, 425: 8−15.
[34] FENG Qi-cheng, WEN Shu-ming, DENG Jiu-shuai, ZHAO Wen-juan. DFT study on the interaction between hydrogen sulfide ions and cerussite (110) surface [J]. Applied Surface Science, 2017, 396: 920−925.
[35] ZHAO Wen-juan, LIU Dian-wen, FENG Qi-cheng, WEN Shu-ming, CHANG Wei-hua. DFT insights into the electronic properties and adsorption mechanism of HS^- on smithsonite (101) surface [J]. Minerals Engineering, 2019, 141: 105846.
[36] LUO Yuan-jia, OU Le-ming, CHEN Jian-hua, ZHANG Guo-fan, JIA Kai. Experimental and DFT study of the sulfidation of smithsonite: Impact of water and oxygen [J]. Applied Surface Science, 2022, 592: 153235.
[37] CHEN Jian-hua. Coordination chemistry of flotation [M]. Beijing: Science Press, 2021. (in Chinese)
[38] CHEN Jian-hua. The interaction of flotation reagents with metal ions in mineral surfaces: A perspective from coordination chemistry [J]. Minerals Engineering, 2021, 17: 107067.
[39] CHEN Jian-hua, ZHU Yang-ge. Study of semi-constrained properties of metal ions on mineral surface of flotation system [J]. Journal of China University of Mining and Technology, 2021, 50(6): 1181−1188. (in Chinese)
[40] DELLEY B. An all-electron numerical method for solving the local density functional for polyatomic molecules [J]. Journal of Chemical Physics, 1990, 92(1): 508−517.
[41] DELLEY B. $DMol^3$ DFT studies: from molecules and molecular environments to surfaces and solids [J]. Computational Materials Science, 2000, 17(2/3/4): 122−126.

白铅矿($PbCO_3$)和菱锌矿($ZnCO_3$)硫化机理的 DFT 研究

陈 晔[1,2]，唐箫琴[3]，陈建华[1]，刘 萌[4]

1. 广西大学 资源环境与材料学院，广西高校矿物工程重点实验室，省部共建特色金属与组合结构全寿命安全国家重点实验室，南宁 530004；
2. 云南省战略金属矿产资源绿色分离与富集重点实验室，昆明 650093；
3. 广西大学 化学化工学院，南宁 530004；
4. 四川大学 化工学院，低碳技术与化学反应工程研究室，成都 610065

摘 要：采用密度泛函理论(DFT)比较研究白铅矿($PbCO_3$)和菱锌矿($ZnCO_3$)硫化机理的差异。通过在 $PbCO_3$/$ZnCO_3$ 表面构建 Pb−S/Zn−S 层来模拟硫化结构。层距和 Mulliken 电荷的结果表明，$PbCO_3$ 上形成稳定的 Pb−S 层，而 $ZnCO_3$ 上形成的 Zn−S 层不稳定。由于 Pb−S 层具有高的共价性，而 Zn−S 层具有高的离子性，因此，硫化−黄药法对 $PbCO_3$ 浮选有效，对 $ZnCO_3$ 浮选无效。为了回收 $ZnCO_3$，需要强离子性捕收剂，因此，硫化−胺法在 $ZnCO_3$ 浮选中应用较广。$PbCO_3$ 和 $ZnCO_3$ 表面硫化层结构和浮选行为差异主要是由于金属离子(Pb^{2+}和 Zn^{2+})和配体(O 配体和 S 配体)极化率的不同以及 Zn^{2+} $3d^{10}$ 轨道的惰性造成的。

关键词：密度泛函理论；白铅矿；菱锌矿；硫化−黄药法；硫化−胺法

(Edited by Bing YANG)